Preprints of the 21st IFAC World Congress (Virtual)
Berlin, Germany, July 12-17, 2020

Person Following from a Nonholonomic Mobile Robot with Ultimately Bounded Tracking Error ⋆

Joël Tari * **Patrick Danès** **

* *LAAS-CNRS, Université de Toulouse, CNRS, UPS*
AKKA Research
Toulouse, France (joel.tari@laas.fr)
** *LAAS-CNRS, Université de Toulouse, CNRS, UPS*
Toulouse, France (patrick.danes@laas.fr)

Abstract: In robotics, "person following" depicts the servoing of the relative situation of a robot w.r.t. a moving person. This property may be hard to achieve, especially when the estimation of the person ego-motion is weak (*e.g.*, due to limited prior knowledge or computational resources). This paper introduces a nonholomic mobile robot controller, which ensures an intuitive and safe behavior through an insightful robot-centered problem statement. Under realistic bounded-error readings of hidden constant person velocities, ultimate boundedness of the state vector norm can be ensured in the neighborhood of its equilibrium.

Keywords: Robotics, Mobile robots, Nonlinear control.

1. INTRODUCTION

Among the developing trends in the collaborative robot industry, the "person following" task has already attracted much attention in fields such as logistics, personal services or collaborative inspection. The aim is to make the robot evolve in the vicinity of a human operator by keeping it servoed on him/her: either leading ahead, moving alongside or lagging behind. Arguably, to perform this task, continuous human motion estimation is required and must be included in the robot motion control algorithm.

What has been seen as the most challenging obstacle and has attracted most contributions is people perception (Dondrup et al., 2015; Linder et al., 2016; Leigh et al., 2015; Montesdeoca et al., 2017). Conversely, the motion control aspect has often been overlooked. Morales et al. (2009) and Leigh et al. (2015) follow the operator from behind by feeding decentralized proportional or PID controllers with the relative translational and rotational errors to the robot. Lagging behind a human is indeed easier as it limits the risk of colliding with obstacles. Leading in front may imply additional planning considerations (Nikdel et al., 2018). However, some use cases require the robot to either navigate alongside the person or to change online its relative distance and angle to him/her. Social acceptance and comfort criteria are studied in Maehara and Fujinami (2018); Shanee et al. (2016).

In view of these considerations, the design of a nonlinear controller enabling a robot to regulate at a constant reference its distance and bearing to a human is hereafter revisited. An approach is proposed, which ensures the exponential stability of the zero-error equilibrium point when the exact person motion is known. To the authors' knowledge, no controller in the literature guarantee properties against unavoidable uncertainties in the assumed velocity of the person. A step towards this aim is done, by showing that the closed-loop system errors converge to a small neighborhood of the origin when subject to pragmatic disturbances on the genuine person velocity.

The paper is organized as follows. Section 2 reviews literature on the control aspect of the "person following task". In Section 3 as the main contribution, a continuous nonlinear feedback controller is proposed that takes into account both the nonholonomic constraint of the robot, and the uncertainty associated with the human motion. Experiments in 4 corroborate its theoretical properties.

2. RELATED WORK

In the literature, person following is addressed along two main control approaches. The inputs to the robot are synthesized so as to control either the relative position of the robot w.r.t. the person frame or the relative position of the person in the robot frame. These approaches are henceforth termed "person frame based control" or "robot centered control", respectively.

2.1 Person Frame Based Control

Given the velocity and orientation of the person in the world frame, Montesdeoca et al. (2017) propose a Lyapunov based controller to position the robot behind him/her at a reference distance. However, in the case when the person is motionless, the design outputs a zero velocity for the robot irrespective of the current error distance, which is unpleasant if the person is waiting for the robot to catch up. In autonomous wheelchair applications, Park and Kuipers (2013) propose a model predictive equilibrium point control. The entailed objective function aims at regulating the robot pose w.r.t. the person frame while

⋆ This work has been partially funded by the French National Research and Technology Agency, in the framework of a CIFRE project involving LAAS-CNRS and AKKA Research.

handling the comfort of surrounding people and avoiding obstacles. The reference pose is reached using the posture stabilization scheme of Park and Kuipers (2011). As noted by Arechavaleta et al. (2006), human locomotion can be viewed as nonholonomic and generally features a faster dynamics compared to a robot. Therefore, if the person velocity changes abruptly, then the reference pose (implicitly coded in the objective function) may jump by a few meters, and thus subsequently lead to an erratic robot behavior. Theoretically, some of these corner cases can be fixed by improving the estimation of the person orientation. However, this would likely require additional computing power for the human perception module. In our opinion, the unpleasant consequences of the uncertainty on the person orientation should be offset by the ability of the controller to provide a safe and intuitive behavior. But as long as the person is cooperative—avoiding corner cases—and the perception module is reliable enough, the person frame based control can be a suitable solution.

2.2 Robot Centered Control

Robot centered control aims at keeping the person in a region defined in the robot frame. The most elementary proportional or PID schemes generate the robot velocities which enable the servocontrol of the person distance in front of the robot (Morales et al., 2009; Leigh et al., 2015). As pointed out by Pucci et al. (2013), the person orientation may be unreliably inferred, so it may be beneficially disregarded. The authors address two major issues: the case when the reference is located on the robot's driving wheels axis, and the so-called jack-knife effect. The first problem is due the nonholomic nature of the robot and has been formulated in a theorem by Brockett (1983) and recalled in Morin and Samson (2008), *i.e.*, no time-invariant continuous state feedback can stabilize the person on the robot driving wheel axis. A discontinuous control solves this issue. The second effect depicts the tendency of the robot to progressively reverse its orientation when the person moves towards it, so that it ends up lagging behind him/her.

3. NONLINEAR FEEDBACK CONTROL

3.1 Definitions

In this section, we firstly assume that the exact velocity of the followed person is known and constant. This strong assumption will be relaxed in Subsection 3.5. The person, also named "target" in the sequel, is described by a single point as his/her orientation (and velocity) is assumed tangent to his/her trajectory in virtue of human motion nonholonomicity (Arechavaleta et al., 2006). Figure 1 sketches the problem and introduces the related notations.

3.2 Kinematics of the Problem

In the fixed frame $\mathcal{F}_0$, the nonholonomic kinematics of the robot are described by

$$\begin{cases} \dot{x} = v\cos\theta & \text{(1a)} \\ \dot{y} = v\sin\theta & \text{(1b)} \\ \dot{\theta} = \omega. & \text{(1c)} \end{cases}$$

Transforming (1) to express the distance and angle from the front of the robot to the target yields the model, defined for $[r, \alpha, \theta]^T \in D =]0; +\infty[\times]\frac{-\pi}{2}, \frac{\pi}{2}[\times \mathbb{R}$,

$$\begin{cases} \dot{r} = -v\cos\alpha - \omega d\sin\alpha & \text{(2a)} \\ \dot{\alpha} = v\dfrac{\sin\alpha}{r} - \omega\Big(\dfrac{d}{r}\cos\alpha + 1\Big) & \text{(2b)} \\ \dot{\theta} = \omega. & \text{(2c)} \end{cases}$$

Let $v_p := [v_{xp}, v_{yp}]^T$ terms the velocity vector of the target T relative to the world ($\mathcal{F}_0$) and expressed in $\mathcal{F}_0$. For $v_p \neq 0$, the state space model (2) extends as:

$$\begin{cases} \dot{r} = -v\cos\alpha + v_{xp}\cos(\alpha+\theta) + v_{yp}\sin(\alpha+\theta) & \text{(3a)} \\ \dot{\alpha} = \dfrac{v}{r}\sin\alpha - \omega - \dfrac{v_{xp}}{r}\sin(\alpha+\theta) + \dfrac{v_{yp}}{r}\cos(\alpha+\theta) & \text{(3b)} \\ \dot{\theta} = \omega. & \text{(3c)} \end{cases}$$

The reference values r^*, α^* entailed in $e = [e_r, e_\alpha]^T$ are assumed constant. The synthesis of the controller is henceforth based on the model

$$\begin{cases} \dot{e} = G(e)u + F(e,\theta)v_p & \text{(4a)} \\ \dot{\theta} = \omega & \text{(4b)} \end{cases}$$

equivalent to (3), with (r and α being respective shortcuts for $e_r + r^*$ and $e_\alpha + \alpha^*$, and the arguments of F, G being omitted for space reasons)

$$G = \begin{bmatrix} -\cos\alpha & -d\sin\alpha \\ \frac{\sin\alpha}{r} & -(1+\frac{d}{r}\cos\alpha) \end{bmatrix}, \quad F = \begin{bmatrix} \cos(\theta+\alpha) & \sin(\theta+\alpha) \\ -\frac{\sin(\theta+\alpha)}{r} & \frac{\cos(\theta+\alpha)}{r} \end{bmatrix}. \quad (5)$$

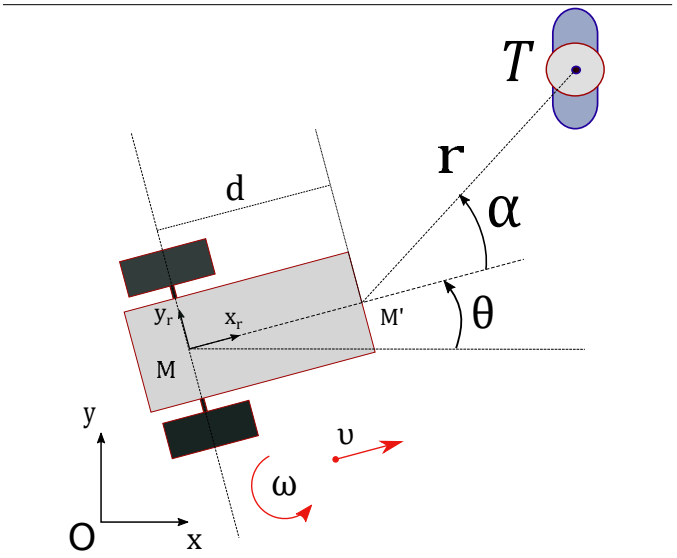

Fig. 1. Definitions (bold symbols term vectors): $\mathcal{F}_0 := (O, \boldsymbol{x}, \boldsymbol{y})$: word frame; $\mathcal{F}_M := (M, \boldsymbol{x}_r, \boldsymbol{y}_r)$: robot frame (with M the robot's drive axle midpoint and $\boldsymbol{x}_r$ orthogonal to this axle); M' foremost point of the robot on $\boldsymbol{x}_r$; $u := [v, \omega]^T$: robot control vector (with v, ω the translational and rotational velocities relative to $\mathcal{F}_0$ and expressed in $\mathcal{F}_M$); $d := \|\boldsymbol{MM'}\|$; $r := \|\boldsymbol{M'T}\|$: distance to the person T; $\alpha := (\widehat{\boldsymbol{x}_r, \boldsymbol{M'T}})$: angle to the person T; $\theta := (\widehat{\boldsymbol{x}, \boldsymbol{x}_r})$: orientation of the robot in $\mathcal{F}_0$; $e := [e_r, e_\alpha]^T := [r - r^*, \alpha - \alpha^*]^T$, with r^*, α^* some reference values; $\tilde{\theta} := \theta - \theta^*$, with θ^* a reference value.

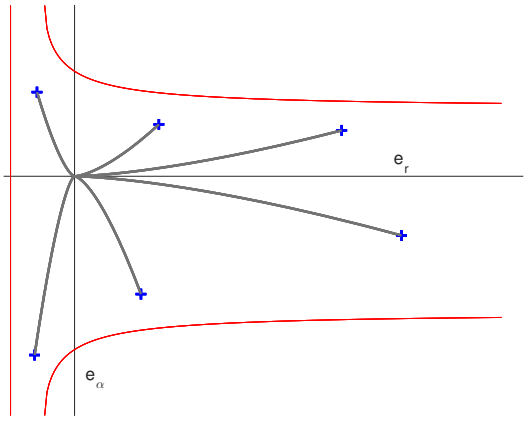

Fig. 2. Phase portrait of subsystem (7b). Several initial conditions are shown in blue. The singularity domain $S = \{e \,|\, e_r = -r^*,\ (e_r + r^*)\cos(\mathrm{e}_\alpha + \alpha^*) + d = 0\}$ is shown in red. In view of the nature of S, the proposed definition (9) leads to a dynamic matrix $A := -P^{-1}Q$ such that any trajectory starting in D_e converges towards the stable node $e = 0$ without making $G(e)$ singular.

3.3 Controller Design

Unless otherwise stated, the target velocity vector v_p is assumed constant. If P and Q are two positive definite matrices of $\mathbb{R}^{2\times 2}$, then the controller

$$u = \left[\begin{smallmatrix} v \\ w \end{smallmatrix}\right] = -G^{-1}(e)P^{-1}\Big(PF(\theta, \mathrm{e})v_p + Qe\Big) \tag{6}$$

linearizes and stabilizes the closed-loop dynamics of subvector e. Indeed, the closed-loop system writes as

$$\begin{cases} \dot\theta = [0\ 1]\, u, & \text{(7a)} \\ \dot e = -P^{-1}Qe & \text{(7b)} \end{cases}$$

where $A := -P^{-1}Q$ satifies $\frac{1}{2}A^TP + \frac{1}{2}PA + Q = 0$.

Fact 1. $G(e)$ is singular, and the feedback system is ill-posed, when $r\cos\alpha = -d$, *i.e.*, if the person is located on the line passing through the driving wheels. This is a direct consequence of Brockett's theorem (Brockett, 1983).

The autonomous closed-loop equation (7b) on e does not make potential singularities of $G(e)$ explicit. As shown by the phase portrait of Figure 2, for general choices of P, Q, there seems to be no guarantee that a trajectory $e(t)$ starting inside the nonsingular domain remains in it. □

To avoid ill-posedness/singularities issues, the control design follows two stages. First, the initial condition domain of $e = [e_r, e_\alpha]^T$ is narrowed to:

$$D_e = \left\{ e \,|\, e_r > -r^*,\ |\,\mathrm{e}_\alpha + \alpha^*| < \arccos\Big(-\frac{d}{(e_r + r^*)}\Big) \right\} \tag{8}$$

Secondly, P and Q are selected such as the dynamic matrix $A := -P^{-1}Q$ of the autonomous linear subsystem (7b) is real diagonal with most negative eigenvalues associated to e_α. To this end, these matrices are set to:

$$P = \left[\begin{smallmatrix} \lambda & 0 \\ 0 & \mu \end{smallmatrix}\right] \text{ and } Q = \mathbb{I}, \text{ with } 0 < \mu < \lambda. \tag{9}$$

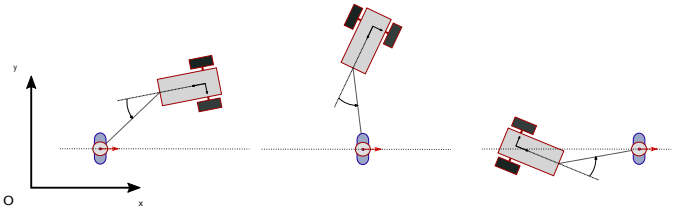

Fig. 3. The jack-knife effect. While keeping the distance and angle to the target at their reference values, the robot progressively retreats behind the person. The equilibrium corresponding to the case when the robot precedes (resp. follows) the person with an absolute orientation of $\pm\pi$ (resp. 0) is unstable (resp. stable).

Fact 2. The origin $e^\diamond = 0$ is the single equilibrium point of the autonomous closed-loop subsystem (7b) and is (locally, in view of ill-posedness issues) asymptotically stable. The closed-loop dynamics of θ thus writes as:

$$\dot\theta = \frac{v_{yp}\cos\theta - v_{xp}\sin\theta + \frac{e_r}{\lambda}\sin\alpha + \frac{re_\alpha}{\mu}\cos\alpha}{d + r\cos\alpha}. \quad \square \tag{10}$$

Define θ^* involved in the definition of $\tilde\theta = \theta - \theta^*$ as

$$\theta^* = \theta^*_k := \mathrm{atan2}(v_{yp}, v_{xp}). \tag{11}$$

Distinct conclusions can be drawn depending on whether the target is static or moving. When the person is static, (*i.e.*, $\forall t \geq t_0,\ v_p(t) = 0$), all possible values for θ are equilibria. When the person moves at constant velocity v_p, one gets

$$\dot{\tilde\theta} = \frac{v_{yp}\cos(\tilde\theta + \theta^*_k) - v_{xp}\sin(\tilde\theta + \theta^*_k) + \frac{e_r}{\lambda}\sin\alpha + \frac{re_\alpha}{\mu}\cos\alpha}{d + r\cos\alpha}. \tag{12}$$

As $\cos\theta^*_k = \epsilon_k \frac{\mathrm{sign}(v_{xp})}{\sqrt{1+v_{yp}^2/v_{xp}^2}}$ and $\sin\theta^*_k = \frac{v_{yp}}{v_{xp}}\cos\theta^*_k$, with $\epsilon_k = +1$ (resp. $\epsilon_k = -1$) for even k (resp. for odd k), the closed-loop system (7b)–(7a) is equivalent to

$$\begin{cases} \dot{\tilde\theta} = f_1(\tilde\theta, e) := \dfrac{(-1)^{k+1}\|v_p\|\sin\tilde\theta + \frac{e_r}{\lambda}\sin\alpha + \frac{re_\alpha}{\mu}\cos\alpha}{d + r\cos\alpha} & \text{(13a)} \\ \dot e = f_2(e) := -P^{-1}Qe, & \text{(13b)} \end{cases}$$

where the following shortcut is used, in addition to $r = e_r + r^*$ and $\alpha = e_\alpha + \alpha^*$:

$$\|v_p\| = \frac{\mathrm{sign}(v_{xp})}{v_{xp}} \frac{v_{xp}^2 + v_{yp}^2}{\sqrt{1+v_{yp}^2/v_{xp}^2}} = \sqrt{v_{xp}^2 + v_{yp}^2}. \tag{14}$$

Hence, the set of equilibrium points of the closed-loop system (7),(13) writes as

$$E = \left\{ [\tilde\theta^\diamond_k, (e^\diamond_k)^T]^T \,|\, e^\diamond_k = 0,\ \tilde\theta^\diamond_k =: \theta^\diamond_k - \theta^*_k = k\pi,\ k \in \mathbb{Z} \right\}. \tag{15}$$

For even k, $[\tilde\theta^\diamond_k, (e^\diamond_k)^T]^T$ is locally asymptotically stable by the Lyapunov first method. Similarly, $[\tilde\theta^\diamond_k, (e^\diamond_k)^T]^T$ is unstable for odd k, which complies with the observed jack-knife effect (Figure 3).

Fact 3. As $f_2(e)$ is Lipschitz and the time-derivative of the Lyapunov function $V(e) = \frac{1}{2}e^TPe$ along the trajectories of (13b) writes as $\dot V(e) = -e^TQe$, the following holds:

$$\forall t \geq 0,\ \|e(t)\| \leq \frac{\lambda_{\max}(P)}{\lambda_{\min}(P)} \exp^{-\frac{1}{2}\frac{\lambda_{\min}(Q)}{\lambda_{\max}(P)}(t-t_0)} \|e(t_0)\|, \tag{16}$$

where the maximum and minimum eigenvalues $\lambda_{\max}(.)$ and $\lambda_{\min}(.)$ simplify in view of the selected P, Q. Besides, the following inequalities hold:

$$c_1\|e\|^2 \leq V_2(e) \leq c_2\|e\|^2,\ \frac{\partial V_2}{\partial e} f_2(e) \leq -c_3\|e\|^2, \quad (17)$$
$$\left\|\frac{\partial V_2}{\partial e}\right\| \leq c_4\|e\|,\ \text{with } c_1=\lambda,\ c_2=c_4=\mu,\ c_3=1. \quad \square$$

3.4 Lyapunov Analysis of the Complete Closed-Loop System

The following unconnected cascade system is first investigated:

$$\begin{cases} \dot{\tilde{\theta}} = f_1(\tilde{\theta}, 0) & (18a) \\ \dot{e} = f_2(e). & (18b) \end{cases}$$

Proposition 4. The function $V_1(\tilde{\theta}) := \frac{1}{2}\tilde{\theta}^2$ is a Lyapunov function for (18) and proves the exponential stability of its equilibrium point $\tilde{\theta}^\diamond = 0$. $\square$

Proof. One has $\forall \tilde{\theta} \neq 0$, $V_1(\tilde{\theta}) > 0$ and $\forall \tilde{\theta} \in [-\theta_a, \theta_a]$, $\dot{V}_1(\tilde{\theta}) = -\frac{\|v_p\|}{d+r^*\cos\alpha^*}\tilde{\theta}\sin\tilde{\theta} < 0$, with $\dot{V}_1(\tilde{\theta})$ the time-derivative of $V_1(\tilde{\theta})$ along the solutions of (18), and $\theta_a \in [-\frac{\pi}{2}, -\pi]$ the solution of $\tan\theta_a + \theta_a = 0$, ($\theta_a \approx 2.04$). In addition, $\dot{V}_1(\tilde{\theta}) \leq -c\tilde{\theta}^2$ holds, with $c := \frac{\|v_p\|}{d+r^*\cos\alpha^*}\frac{\sin\theta_a}{\theta_a}$, what concludes the proof [1]. $\square$

Inspiring from (Khalil, 2014, Appendix C), and considering the closed-loop system (13), the exponential stability of the origin can be proved on the basis of $V_1(\tilde{\theta})$ and $V_2(e)$ defined above.

Theorem 5. If there exists a Lipschitz constant L_Ω such that $\forall [\tilde{\theta}, e^T]^T \in [-\theta_a, \theta_a] \times \Omega$, with $\Omega \in D_e$ a closed set centered around the origin,

$$\left\|\frac{\partial V_1}{\partial \tilde{\theta}}\big(f_1(\tilde{\theta}, e) - f_1(\tilde{\theta}, 0)\big)\right\| \leq L_\Omega\|e\| \quad (19)$$

holds, then the equilibrium $[(\tilde{\theta}^\diamond), (e^\diamond)^T]^T = 0$ of (13) is exponentially stable. $\square$

Proof. Define

$$V(\tilde{\theta}, e) = bV_1(\tilde{\theta}) + V_2(e),\ b > 0. \quad (20)$$

Then, $\dot{V}(\tilde{\theta}, e) = b\frac{\partial V_1}{\partial \tilde{\theta}} f_1(\tilde{\theta}, 0) + b\frac{\partial V_1}{\partial \tilde{\theta}}\big[f_1(\tilde{\theta}, e) - f_1(\tilde{\theta}, 0)\big] + \frac{\partial V_2}{\partial e} f_2(e)$ can be upper bounded by

$$\dot{V}(\tilde{\theta}, e) \leq -bc\|\tilde{\theta}\| + bL\|\tilde{\theta}\|\|e\| - c_3\|e\|^2 =: -\begin{bmatrix}\|\tilde{\theta}\| \\ \|e\|\end{bmatrix}^T S \begin{bmatrix}\|\tilde{\theta}\| \\ \|e\|\end{bmatrix},$$
$$\text{with } S := \begin{bmatrix} bc & -bL/2 \\ -bL/2 & c_3 \end{bmatrix}. \quad (21)$$

Selecting $b < 4cc_3/L^2$ ensures that $\dot{V}(\tilde{\theta}, e)$ is negative definite on $[-\theta_a, \theta_a] \times \Omega$ and that $[(\tilde{\theta}^\diamond), (e^\diamond)^T]^T = 0$ is exponentially stable. $\square$

Note that equivalently, the constant L_Ω must be greater than $\frac{1}{\sqrt{e_r^2+e_\alpha^2}}\left|\|v_p\|\sin\tilde{\theta}\left(\frac{1}{d+r^*\cos\alpha^*} - \frac{1}{d+r\cos\alpha}\right) + \frac{\frac{e_r}{\lambda}\sin\alpha + \frac{re_\alpha}{\mu}\cos\alpha}{d+r\cos\alpha}\right|$ for all $[\tilde{\theta}, e^T]^T$ in $[-\theta_a, \theta_a] \times \Omega$. The following more conservative condition can be imposed on L_Ω by using the triangular inequality, which allows the removal of $\sin\tilde{\theta}$:

$$\frac{\|v_p\|\left|\frac{1}{d+r^*\cos\alpha^*} - \frac{1}{d+r\cos\alpha}\right| + \left|\frac{1}{d+r\cos\alpha}\left(\frac{e_r}{\lambda}\sin\alpha + \frac{re_\alpha}{\mu}\cos\alpha\right)\right|}{\sqrt{e_r^2+e_\alpha^2}} \leq L_\Omega. \quad (22)$$

[1] In fact, $\dot{V}_1 < 0$ on $]-\pi, \pi[$ and admits an inflexion point at θ_a.

As will be shown in the experiments section, L_Ω is determined on a per case basis.

3.5 Uncertain Target Velocities

In practice, the velocity vector of the target is not perfectly known. So, the controller (6) and the closed-loop system (13) respectively become

$$u = -G^{-1}(e)P^{-1}\Big(PF(\tilde{\theta}, e)\hat{v}_p + Qe\Big) \quad (23)$$

with $\hat{v}_p$ the estimate of v_p and

$$\begin{cases} \dot{\tilde{\theta}} = \dfrac{(-1)^k\|\hat{v_p}\|\sin\tilde{\theta} + \frac{e_r}{\lambda}\sin\alpha + \frac{re_\alpha}{\mu}\cos\alpha}{d + r\cos\alpha} & (24a) \\ \dot{e} = -P^{-1}Qe + F(\tilde{\theta}, e)\big(v_p - \hat{v}_p\big). & (24b) \end{cases}$$

Theorem 6. $e = 0$ is no longer an equilibrium point—nor a partial equilibrium in the sense of Vorotnikov and Martyshenko (2010)—of the perturbed subsystem (24b). Its dynamics depends on $\tilde{\theta}$. However, if the norm $\|v_p - \hat{v}_p\|$ is uniformly upper bounded at all times, then ultimate boundedness of the state vector $[\tilde{\theta}^T, e^T]^T$ of (24) is in effect. $\square$

Proof. Assume that there exists $\gamma > 0$ such that $\forall t > t_0, \|v_p - \hat{v}_p\| \leq \gamma$. Then, for all r in $[r_{\min}, +\infty]$, $r_{\min} > 0$, $\|F(\tilde{\theta}, e)(v_p - \hat{v}_p)\| \leq \delta$ holds, with $\delta := \gamma \sup\|F(\tilde{\theta}, e)\| = \gamma\max(1, 1/r_{min})$. From the properties defined in subsection 3.4, there exist constants h_1, h_2, h_3, h_4 such that, for $\big[\tilde{\theta}, e^T\big]^T \in \mathcal{B}_\rho$, the ball centered on 0 of radius ρ:

$$h_1\left\|\big[\tilde{\theta}, e^T\big]^T\right\|^2 \leq V(\tilde{\theta}, e) \leq h_2\left\|\big[\tilde{\theta}, e^T\big]^T\right\|^2,$$
$$\frac{\partial V}{\partial \tilde{\theta}} f_1(\tilde{\theta}, e) + \frac{\partial V}{\partial e} f_2(e) \leq -h_3\left\|\big[\tilde{\theta}, e^T\big]^T\right\|^2, \quad (25)$$
$$\left\|\left[\frac{\partial V}{\partial \tilde{\theta}}, \Big(\frac{\partial V}{\partial e}\Big)^T\right]^T\right\| \leq h_4\left\|\big[\tilde{\theta}, e^T\big]^T\right\|.$$

Define

$$\mathcal{C} := \frac{h_3}{h_4}\sqrt{\frac{h_1}{h_2}} = \frac{\nu}{\max(b, \mu)}\sqrt{\frac{\min(b, \lambda)}{\max(b, \mu)}}, \quad (26)$$

with ν the maximum eigenvalue of S. Define z such that $0 < z < 1$. If, for all $t \geq t_0$ and $\big[\tilde{\theta}, e^T\big]^T \in \mathcal{B}_\rho$, $\delta < \mathcal{C}z\rho$ holds, then, for all trajectories starting in domain $\Big\{V(\tilde{\theta}, e) \leq h_1\rho^2\Big\}$, the ultimate boundedness lemma defined in (Khalil, 2014, Lemma 4.3) applies, and leads to the following upper bound on the solution :

$$\left\|\big[\tilde{\theta}(t), e^T(t)\big]^T\right\| \leq \max\left\{\eta\exp\Big(-\frac{t-t_0}{\tau}\Big)\left\|\big[\tilde{\theta}(t_0), e^T(t_0)\big]^T\right\|, \frac{\delta}{z\mathcal{C}}\right\}.$$
$$\text{with } \eta := \sqrt{h_2/h_1},\ \ \tau := \frac{2h_2}{h_3(1-z)} \quad (27)$$

Exponential convergence of the norm of the state vector is guaranteed towards a domain around 0 all the smaller as uncertainties on the velocity are low. $\square$

4. EXPERIMENTS

We conduct a real world experiment using a differential drive robot equipped with 2d laser range scanner to evaluate our controller. The robot used in our setting is the AirCobot differential drive robot (Jovančević et al., 2015).

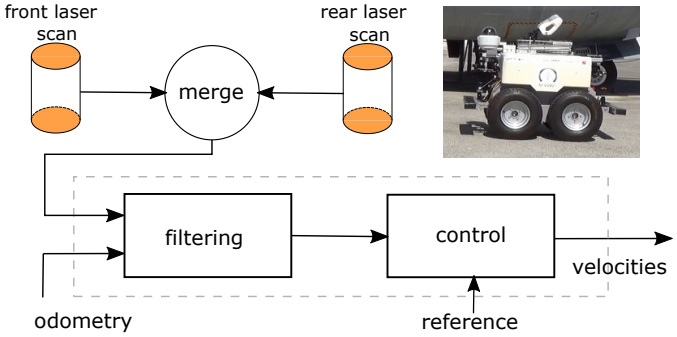

Fig. 4. Block diagram of the follower system.

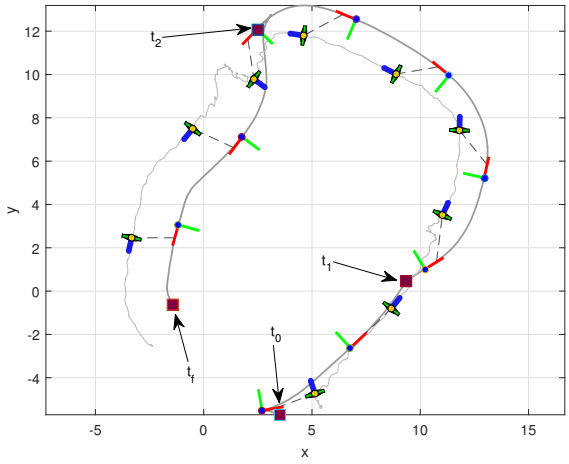

Fig. 5. Trajectory of the robot (RGB frames) and the person followed during the experiment

Among the sensors available on the platform, we use 2 Hokuyos UTM-30LX scanning ahead and behind, at knees level. The robot velocities are saturated in practice at 1.35 m/s for the translational velocity and 0.4 rad/s for the rotational velocity. The embedded computer is an intel i7 3.2Ghz with 32Go RAM. Our follower module is implemented in a C++ package wrapped into the popular ROS middleware. Its state machine is controlled by a tablet application, enabling the person followed to change online the angle-distance reference.

Figure 4 summarizes the architecture of the follower module implementation. Target positions and velocities are inferred by mean-clustering the laser points at 40Hz in a search region given the last position of the target in the fixed world frame. The velocities are subsequently computed using a linear least squares model over the last 50 readings.

Figure 5 shows the achieved trajectory. The robot objective is to follow the target on time segment $[t_0, t_1]$ with references $(r^* = 2, \alpha^* = 0)$, on $[t'_1, t_2]$ with $(r^* = 2, \alpha^* = 0.8727)$ and on $[t'_2, t_f]$ with $(r^* = 2, \alpha^* = -1.309)$. The module of the target velocity is considered constant within each segment: $\hat{v_{p_1}} := 0.6m/s$, $\hat{v_{p_2}} := 0.75m/s$, $\hat{v_{p_3}} := 0.65m/s$. The upper bound on the velocity norm error is set as: $\gamma = 0.4m/s$. Other constants are set during the whole setup as: $\mu = 1$, $\lambda = 1.4$, $r_{min} = 0.4m$, $z = 0.75$ and $\rho = 1.5$. μ, λ and r_{min} are robot-specific and could have been chosen otherwise for a more agile platform. Recall that ρ defines the radius of the ball onto which $\left[\tilde{\theta}, e^T\right]^T$ must live for theorem 6 to be valid. Therefore, a small value set for ρ would be impractical.

Table 1. Ultimate boundedness of solutions for time sequences

Time segment	$\alpha^*(rad)$	L_Ω	Ultimate bound
$[t_0, t_1]$	0	1.2	0.336
$[t'_1, t_2]$	0.8727	2	0.51
$[t'_2, t_f]$	-1.309	1.1	0.2906

Table 1 shows the expected ultimate bounds values as well as the constants complying with the Lipschitz condition, one example being shown in Figure 7 for the first time segment. Results are displayed on Figure 6. The ultimate bounds under hypothesis $\gamma = 0.4$ are achieved on the three segments when the target velocity is close to constant. Out of bounds cases were noticeable during a rapid change of course of the followed person, because his/her measured velocity exceeded the hypothesized value γ. During segments $[t_1, t'_1]$ and $[t_2, t'_2]$, the target stops to change angle-distance references. The component $\tilde{\theta}$ displays large errors at stops, but those situations have no relevance since no stable equilibrium can be set for $\|v_p\| = 0$ as stated in (11). Furthermore, the quite restrictive robot rotational velocity saturation has not been integrated in our model. Its effect is notable. Except for these cases, the norm of the error is bounded as expected under our hypothesis, despite the human perception module having achieved rather erratic positioning (Figure 5) and velocity (Figure 6).

5. CONCLUSION

A new state feedback controller has been proposed for the person follower problem within the robot centered paradigm. The solution acknowledges at the control level the detrimental effects of the uncertainty associated with the person speed and direction, what had not been done before. For an assumed an upper bound on the person velocity estimation errors, the system state is ultimately trapped in a ball of given radius around the origin.

The solution could then be extended to avoid obstacles by moving the equilibrium as done by (Park and Kuipers, 2013), with the added benefit that the distance between the robot and the person would still be guaranteed at the controller level, without resorting to motion planning.

A perspective could consist in addressing the non-constant target velocity case, by proving exponential stability of the origin of the time-varying counterpart of (13). But currently, as a uniform small bound on the norm $\|v_p(t) - \hat{v}_p(t)\|$ can be hardly found when the person ego-motion changes, no relevant ultimate bound can be proved.

REFERENCES

Arechavaleta, G., Laumond, J., Hicheur, H., and Berthoz, A. (2006). The nonholonomic nature of human locomotion: a modeling study. In *IEEE/RAS-EMBS*

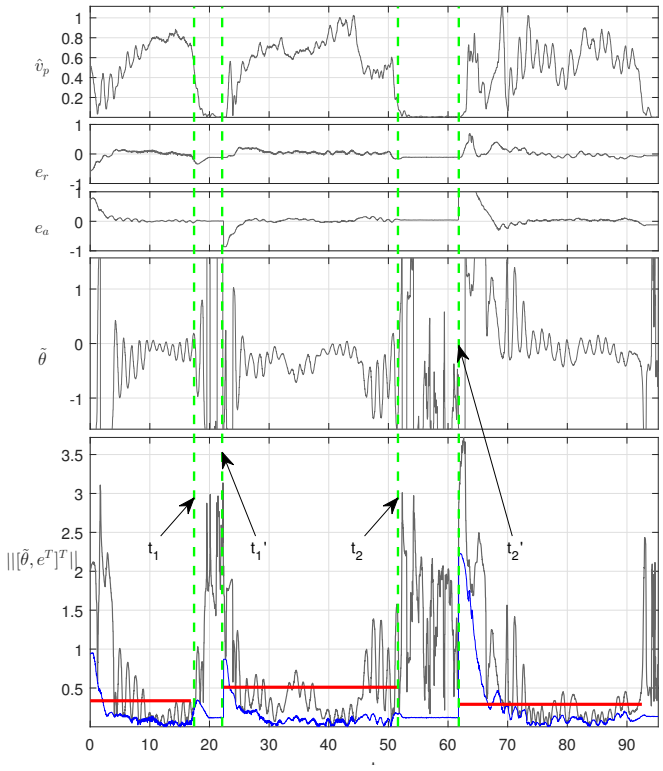

Fig. 6. From top to bottom: estimated target velocity $\|\hat{v_p}\|$,e_r,e_a and $\tilde{\theta}$. At the bottom, norm $\left\|\left[\tilde{\theta}(t), e^T(t)\right]^T\right\|$ is shown (black) as well as norm $\|e\|$ (blue). Expected ultimate bounds are shown within their respective time segments (red).

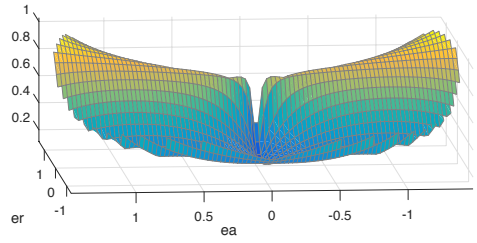

Fig. 7. The surface $\frac{\|f1(\tilde{\theta},e)-f(0,e)\|}{\|e\|}$ complies with a Lipschitz $L_\Omega := 1.2$ constant upper bound.

Int. Conf. on Biomedical Robotics and Biomechatronics (BioRob'2006). Pisa, Italy.

Brockett, R. (1983). Asymptotic stability and feedback stabilization. In R. Brockett, R. Millman, and H. Sussmann (eds.), *Differential Geometric Control Theory*, 181–208. Birkhauser, Boston.

Dondrup, C., Bellotto, N., Jovan, F., and Hanheide, M. (2015). Real-time multisensor people tracking for human-robot spatial interaction. *IEEE Int. Conf. on Robotics and Automation (ICRA'2015)*.

Jovančević, I., Orteu, J., Sentenac, T., and Gilblas, R. (2015). Automated visual inspection of an airplane exterior. In F. Meriaudeau and O. Aubreton (eds.), *Proceedings of SPIE 9534*, 95340Y. Le Creusot, France.

Khalil, H. (2014). *Nonlinear Control*. Pearson Education Limited.

Leigh, A., Pineau, J., Olmedo, N., and Zhang, H. (2015). Person tracking and following with 2D laser scanners. In *IEEE Int. Conf. on Robotics and Automation (ICRA'2015)*. Seattle, WA.

Linder, T., Breuers, S., Leibe, B., and Arras, K.O. (2016). On multi-modal people tracking from mobile platforms in very crowded and dynamic environments. In *IEEE Int. Conf. on Robotics and Automation (ICRA'2016)*, 5512–5519. Stockholm, Sweden.

Maehara, K. and Fujinami, K. (2018). Psychological Effects on Positional Relationships Between a Person and a Human-Following Robot. In *IEEE Int. Conf. on Embedded and Real-Time Computing Systems and Applications (RTCSA'2018)*. Hakodate, Japan.

Montesdeoca, J., Toibero, M., and Carelli, R. (2017). Person-following based on social navigation into the sensorized environments. In *IEEE Int. Conf. on Robotics and Biomimetics (ROBIO'2017)*. Macau, China.

Morales, J., Martínez, J., Martínez, M., and Mandow, A. (2009). Pure-Pursuit reactive path tracking for nonholonomic mobile robots with a 2d laser scanner. *EURASIP Jour. on Advances in Signal Processing*, 2009, 1–10.

Morin, P. and Samson, C. (2008). *Motion Control of wheeled mobile robots*. Springer.

Nikdel, P., Shrestha, R., and Vaughan, R. (2018). The Hands-Free Push-Cart: Autonomous following in front by predicting user trajectory around obstacles. In *IEEE Int. Conf. on Robotics and Automation (ICRA'2018)*. Brisbane, Australia.

Park, J. and Kuipers, B. (2011). A smooth control law for graceful motion of differential wheeled mobile robots in 2d environment. In *IEEE Int. Conf. on Robotics and Automation*. Shanghai, China.

Park, J. and Kuipers, B. (2013). Autonomous person pacing and following with Model Predictive Equilibrium Point Control. In *IEEE Int. Conf. on Robotics and Automation (ICRA'2013)*. Karlsruhe, Germany.

Pucci, D., Marchetti, L., and Morin, P. (2013). Nonlinear control of unicycle-like robots for person following. In *IEEE/RSJ Int. Conf. on Intelligent Robots and Systems (IROS'2013)*. Tokyo, Japan.

Shanee, H.S., Dror, K., Tal, O.G., and Yael, E. (2016). The influence of following angle on performance metrics of a human-following robot. In *IEEE Int. Symp. on Robot and Human Interactive Communication (ROMAN'2016)*, 593–598. New York, NY.

Vorotnikov, V. and Martyshenko, G. (2010). On partial stability theory of nonlinear dynamic systems. *Jour. of Computer and System Sciences International*, 49(5), 702–709.